JOURNAL OF GEOPHYSICAL RESEARCH, VOL. 105, NO. A8, PAGES 18,483–18,493, AUGUST 1, 2000

On the magnetospheric source regions of substorm-related field-aligned currents and auroral precipitation

G. Lu

High Altitude Observatory, National Center for Atmospheric Research, Boulder, Colorado

M. Brittnacher and G. Parks

Department of Geophysics, University of Washington, Seattle

D. Lummerzheim

Geophysical Institute, University of Alaska, Fairbanks

Abstract. This paper presents a detailed analysis of field-aligned currents and auroral UV emissions during an isolated substorm on January 9, 1997. The large-scale upward field-aligned currents derived from the assimilative mapping of ionospheric electrodynamics (AMIE) procedure are found to generally coincide with the relatively intense auroral emissions in the central auroral oval, and downward field-aligned currents are mostly in the poleward edge (and with much weaker downward currents at the equatorward edge) of the auroral oval where auroral luminosity is considerably lower. However, the brightest, yet localized, discrete auroras shown in the UV images often lie at the boundary between upward and downward field-aligned currents, indicating that the current AMIE spatial resolution is unable to resolve the fine-scale filamentary field-aligned currents that are expected to be associated with the localized auroral features. The initial auroral brightening at the substorm onset occurs near the midnight region; intense auroral precipitation then appears to shift toward dusk and to higher latitudes in the ionosphere as the substorm proceeds. Using an improved time-dependent magnetic field model specified for this event, we find that the initial auroral intensification at the substorm onset maps to the inner central plasma sheet between -5 and -7 R_E, with its earthward edge located just outside of the plasmapause. During the substorm expansion phase, the corresponding magnetospheric source region of auroral precipitation moves slightly tailward and toward the dusk flank near the low-latitude boundary layer. At the late stage of the expansion phase, bright discrete auroras map to a narrow region of tailward plasma convection that is embedded in a wide and predominantly earthward convection zone. The mapping of substorm-related field-aligned currents, on the other hand, is more confined close to the Earth, with the current density peaks around geosynchronous altitude. The apparently different magnetospheric source regions imply that the processes that produce energetic precipitating particles are not the same ones that generate the strongest magnetic perturbations in the magnetosphere. The relative importance of electrostatic fields and the inductive electric fields during the substorm expansion phase is also investigated. It is shown that the inductive electric fields are comparable to or even larger in magnitude than the electrostatic fields at the early expansion phase, but they become less important at the late stage of the substorm expansion phase.

1. Introduction

The most easily observed substorm activity is the intensification of auroral emissions in the ionosphere. Enhanced auroral precipitation during substorms can increase ionospheric conductivity dramatically, and hence increase ionospheric currents over the auroral zone. Field-aligned currents, especially upward field-aligned currents, are considered to be carried mostly by electrons. It therefore would be natural to expect field-aligned currents and auroral precipitation to display coherent variations during substorms. With the help of satellite-borne imagery, global auroral activity can be monitored closely during substorms. However, global

Paper number 1999JA000365.
0148-0227/00/1999JA000365$09.00

instantaneous distribution of field-aligned current is still relatively difficult to obtain due to the lack of sufficient global observations of electric fields or ionospheric convection. So far, global-scale studies of field-aligned currents with respect to auroral precipitation during substorms are conducted mainly through superposition of many individual satellite passes during different substorm events [e.g., *Fujii et al.*, 1994; *Marklund et al.*, 1998].

One of the key issues concerning substorms is to understand where in the magnetosphere auroral precipitating particles and field-aligned currents project to. Over the past two decades, studies have linked intense auroras to the different regions in the magnetosphere, from the inner edge of the central plasma sheet (CPS) [e.g, *Lui and Burrows*, 1978; *Feldstein and Galperin*, 1985; *Samson et al.*, 1992] to the low-latitude boundary layer (LLBL) [*Rostoker and Eastman*, 1987; *Eastman et al.*, 1988]. By examining the Viking UV auroral images and mapping them to the magnetosphere using the T87 magnetic field model [*Tsyganenko*, 1987], *Elphinstone et al.* [1993] concluded that during quiet times nightside auroral arcs map to the region earthward of -15 R_E, whereas during the late substorm expansion phase or early recovery phase the nightside LLBL becomes an important source region of auroral precipitation. Views on the magnetospheric source regions of substorm-related field-aligned currents are even more diverse. Since it is practically impossible to reconstruct the global magnetospheric current distributions during substorms from all available satellite observations, these different views are, to some extent, influenced by the different substorm models that people have put forth. For instance, the current disruption model [*Lui*, 1996, and references therein] attributes the collapse of intense cross-tail currents near the inner edge of the plasma sheet inside of -12 R_E to the formation of the substorm current wedge. The boundary layer model [*Rostoker*, 1996, and references therein] also associates expansion phase onset with the collapse of the near-Earth cross-tail current typically earthward of -12 R_E across the midnight sector. This initial collapse progresses tailward and stimulates reconnection somewhere 20~40 R_E behind the Earth. The enhanced earthward convective flow associated with this reconnection stimulates the Kelvin-Helmholtz instability (KHI) on closed field lines in the velocity shear zone between the low-latitude boundary layer and the central plasma sheet. Field-aligned currents flow out of the dawnside velocity shear and into the duskside velocity shear in the plasma sheet. Along with the enhanced westward ionospheric electrojets, they form the three-dimensional substorm current system. The ionospheric response to the KHI is marked by substorm intensifications near the poleward edge of the auroral oval along the evening sector high-latitude convection reversal (which maps to the LLBL-CPS interface). The near-Earth neutral line model [e.g., *Baker et al.*, 1996, and references therein] proposes that the enhanced reconnection in the midtail and far-tail regions is the primary cause of field-aligned currents during substorms. However, recently MHD simulations [*Birn and Hesse*, 1996] and satellite observations [*Shiokawa et al.*, 1998] suggest that reconnection in the midtail region leads to earthward bursty bulk flows which transfer energy and magnetic flux to the near-Earth region where field-aligned currents develop as a consequence of the braking of the earthward flows.

In this paper we investigate the instantaneous relationship between auroral precipitation and large-scale field-aligned currents in the ionosphere during the expansion phase of a substorm on January 9, 1997. We further show the magnetospheric mapping of the substorm-related auroral precipitation and field-aligned currents to shed new light on their magnetospheric source regions.

2. Results

The January 9, 1997, substorm was a relatively simple and isolated event due to the fact that the interplanetary magnetic field (IMF) was weak but steady. The solar wind conditions as well as the auroral electrojet indices are shown in Figure 1 (adapted from *Lu et al.* [1999]). According to the 5-min-resolution *AL* index, the substorm growth phase started at ~0600 UT, the onset of the expansion phase was at ~0745 UT, and the recovery phase began at ~0840 UT. The minimum *AL* value was about -400 nT, corresponding to a moderate substorm activity level. The *Dst* index was nearly constant, with an average value of ~2 nT.

Plate 1 shows Polar UV auroral images overlapped with field-aligned currents at selected UT times during the substorm expansion phase. The images were obtained using the Lyman-Birger-Hopfield longer wavelength (denoted LBHl) filter so that the auroral luminosity was directly proportional to the energy flux of precipitating electrons [*Brittnacher et al.*, 1999]. Owing to satellite wobble, the Polar UV images suffer a degradation in the direction perpendicular to the satellite track. The single-pixel spatial resolution of the ultraviolet imager (UVI) projected to 120 km altitude is nominally about 40×40 km near apogee. However, spacecraft wobble motion degrades this resolution to 40×400 km, with the longer dimension approximately in the noon-midnight direction on this date. Recently, Bayesian image reconstruction which applies the Pixon algorithm (see for details, M. Brittnacher et al., Large-scale structure of dayside poleward moving aurora for $B_y > 0$, submitted to *Geophysical Research Letters*, 2000) has been used to restore the original resolution, although some residual wobble effects may still be present. The images shown in Plate 1 are wobble-corrected and they have a spatial resolution of 40×80 km. Field-aligned currents were derived based on 1-min-averaged ground magnetometer data along

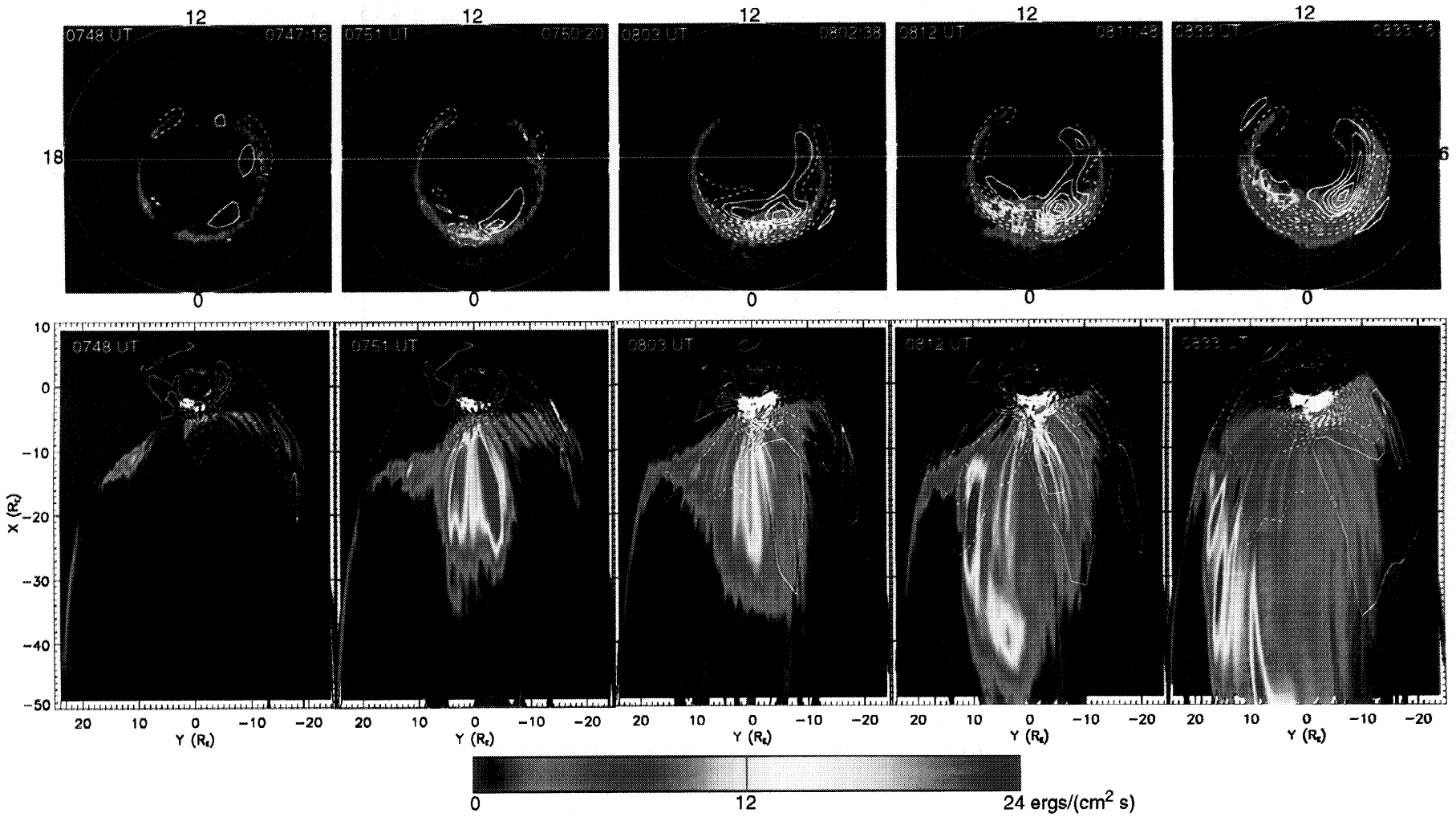

Plate 1. (top) Distributions of auroral UV emissions and field-aligned currents at selected times during the substorm expansion phase on January 9, 1997. (bottom) Corresponding equatorial maps of auroral UV emissions and field-aligned currents. The solid contours represent currents that flow into the ionosphere, and the dashed contours represent currents flowing out of the ionosphere. The contour interval is 0.3 μA/m^2 for the ionospheric maps and 0.1 nA/m^2 for the equatorial maps.

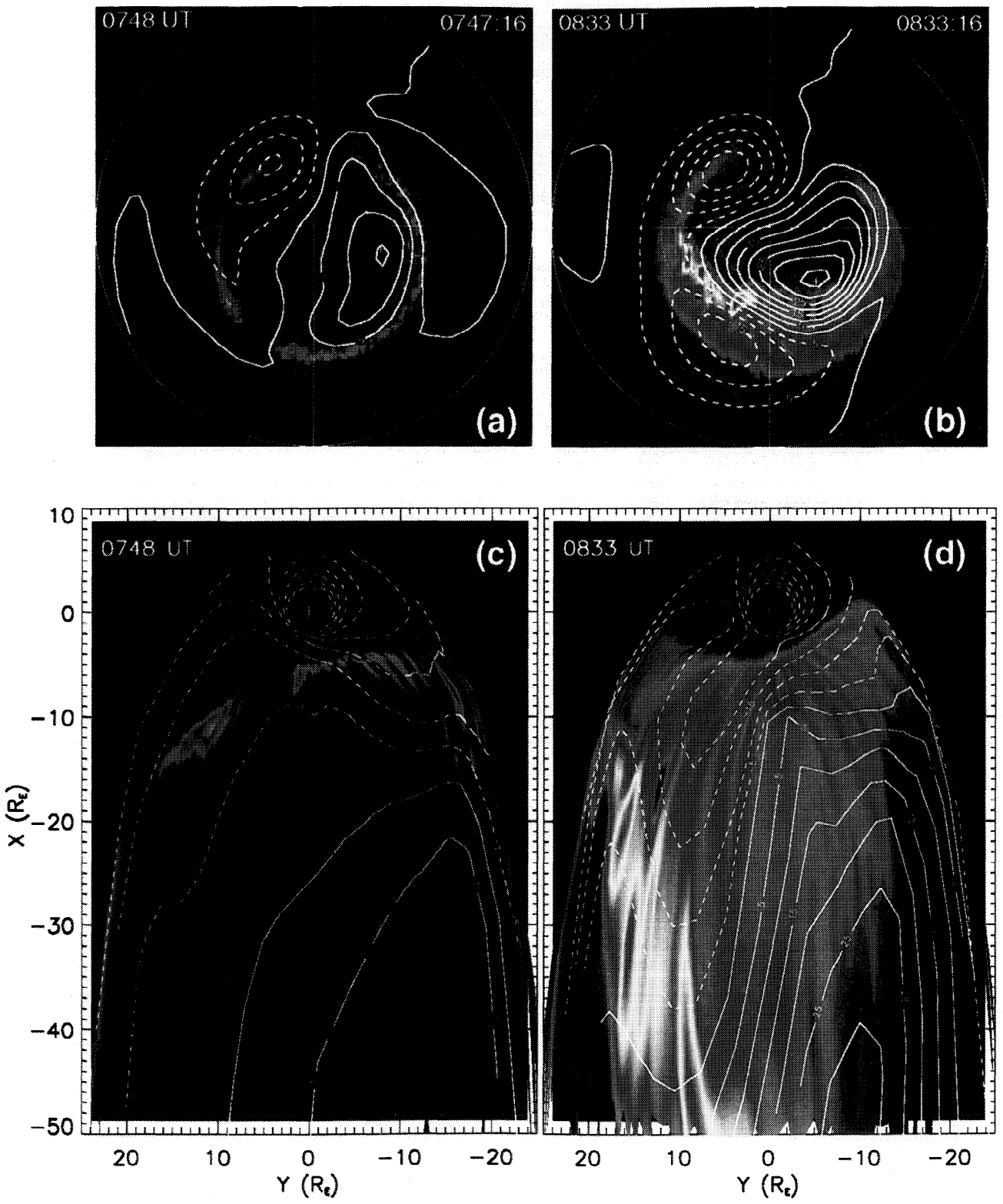

Plate 2. Distributions of auroral UV emissions and plasma convection (a) in the polar ionosphere at the beginning of the substorm expansion phase, (b) in the polar ionosphere near the end of the substorm expansion phase, (c) in the equatorial magnetosphere at the beginning of the substorm expansion phase, and (d) in the equatorial magnetosphere near the end of the substorm expansion phase.

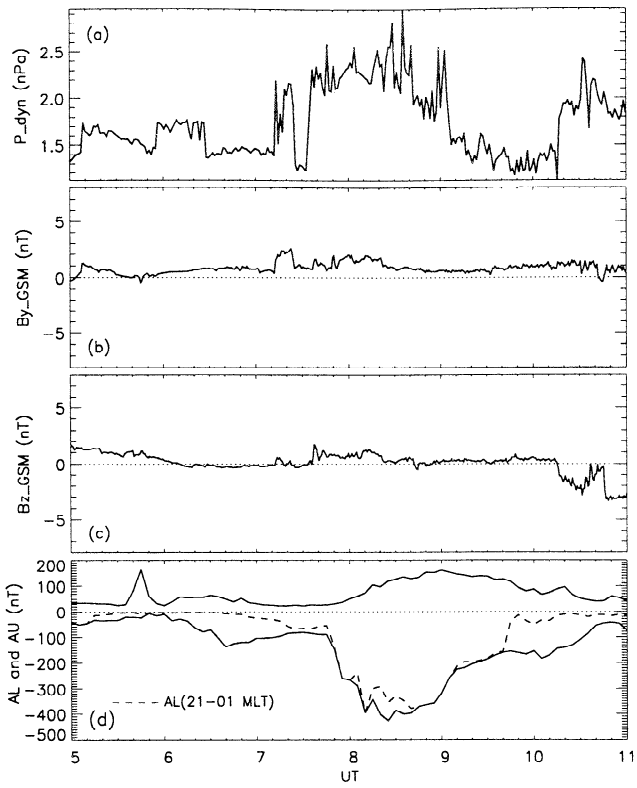

Figure 1. (top to bottom) Solar wind dynamic pressure, the IMF B_y and B_z components in GSM coordinates, and the auroral electrojet indices AU and AL between 0500 and 1100 UT on January 9, 1997. A time delay of 21 min has been applied to the Wind satellite data.

with the global auroral images from the Polar UVI, using the assimilative mapping of ionospheric electrodynamics (AMIE) procedure [*Richmond and Kamide*, 1988]. Height-integrated Pedersen and Hall conductivities were estimated from a pair of Polar UV images [*Lummerzheim et al.*, 1997] at every 3 min. Note that the Polar UV images used in deriving the height-integrated conductances were not corrected for the wobble effects. The AMIE procedure currently has a grid size of 1.7° in latitude and 10° in longitude. The use of the wobbled UV images in AMIE further smears out the small-scale structures of field-aligned currents in the noon-midnight direction. Ideally, we would like to use an independent data source for estimating the ionospheric conductances since they have a strong influence on the AMIE-derived field-aligned currents. Unfortunately, global auroral images currently are the only way to obtained global, instantaneous distributions of auroral conductances, although this method is subject to uncertainties regarding where in the atmosphere auroral emissions are excited [*Lummerzheim et al.*, 1997]. Nevertheless, we believe that the ionospheric conductances based on Polar UV images are much more reliable than any existing statistical models, and field-aligned currents derived from AMIE for this study are relatively reliable in terms of large-scale structures. However, there are no observations available that could be used to corroborate our estimation of field-aligned currents.

The substorm onset was first captured by the Polar UVI at 0747:16 UT, followed by major auroral intensification, a manifestation of the substorm expansion phase. A smaller brightening, seen much earlier at ~0719 UT, was attributed to a pseudobreakup [*Brittnacher et al.*, 1999]. The UV images shown in Plate 1 were taken within 1 min of the corresponding AMIE field-aligned current patterns. Although more intense emissions were seen near ~2000 MLT and on the dawnside at the onset, they appeared to be the residual activity from the earlier pseudobreakup. During the expansion phase the nightside emission intensified and also moved gradually poleward as well as westward toward dusk.

The distributions of field-aligned currents are shown as contours in Plate 1, with the solid contours representing downward currents that flow into the ionosphere and the dashed contours representing upward currents flowing out of the ionosphere. At 0748 UT, right after the onset, the large-scale distribution showed a pair of region 1 and region 2 currents on the dawnside, but showed only the upward region 1 currents on the duskside. Downward field-aligned currents were also found in the postmidnight sector. By 0751 UT the dayside field-aligned currents had diminished, whereas a pair of field-aligned currents with the nightside region 1 polarity near midnight had intensified significantly. This pair of field-aligned currents formed the so-called substorm wedge currents [*McPherron et al.*, 1973], and the peaks of field-aligned currents were oriented roughly in the east-west direction and were closed in the ionosphere through the enhanced westward electrojets [*Lu*, 2000]. The nightside field-aligned currents continued to grow during the expansion phase, not only in intensity, but also in spatial extension. It is worth pointing out that the AMIE results show clearly that the nightside field-aligned currents related to the substorm activity are not merely the distortion of preexisting region 1 and region 2 currents; rather, they are a separate current system initiated near midnight after the substorm onset [*Lu*, 2000]. As shown in the top images of Plate 1, the large-scale upward field-aligned currents generally coincided with the bright auroras in the central auroral oval; the majority of the downward field-aligned currents were found at the poleward edge of the auroral oval, but much weaker downward currents were also seen at the equatorward edge, where auroral emissions were considerably lower. However, the brightest, yet more localized, auroral emissions tend to reside at the boundary between upward and downward currents. This probably is not surprising since the brightest discrete auroras are often associated with intense filamentary upward currents. However, the coarse grid nature of the AMIE patterns precludes the representation of such small-scale structures.

The bottom images of Plate 1 show the corresponding mapping of auroral images and field-aligned currents in the magnetospheric equatorial plane by using the time-dependent magnetic field model specified for this case (see *Lu et al.* [1999] for a detailed description of the model). The mapping of auroral precipitation is conducted through direct field line tracing, in the same fashion as *Elphinstone et al.* [1993] and *Pulkkinen et al.* [1995, 1998]. The mapping of field-aligned currents, on the other hand, has to take into account a geometric mapping factor. Assuming there is no current leakage across the field lines from the ionosphere to the equatorial magnetosphere, the current density is then scaled by the factor of B_e/B_i, where B_e and B_i are the magnetic field strength at the equator and in the ionosphere, respectively. The equatorial maps show that substorm-related auroral precipitation was initiated in the central plasma sheet and the inner edge of the precipitation region was at $X \sim -5\ R_E$ tailward of the Earth at the substorm onset.

As the substorm progressed, the corresponding magnetospheric source region moved tailward and also moved gradually toward the dusk flank. At 0748 UT the mapped field-aligned currents of the nightside region 2 polarity were found around $L = 4$, with currents flowing into the ionosphere (solid contours) on the dawnside of the midnight meridian and flowing out of the ionosphere (dashed contours) on the duskside. Field-aligned currents tailward of -4 R_E and near the midnight meridian were primarily flowing out of the ionosphere even though they were too weak to show up in the corresponding ionosphere. The downward field-aligned currents shown in the postmidnight sector in the ionosphere, however, became very weak when mapped to the equatorial plane due to the fact that they were at higher latitudes so that the mapping factor became relatively small. At 0751 UT, though the pair of substorm wedge currents became very evident in the ionosphere, only the upward currents at relatively lower latitudes were shown in the equatorial plane. The wedge-type current distribution was not seen in the equatorial plane until during the late expansion phase after about 0800 UT. These wedge-type field-aligned currents seemed to have a wider extent in the y direction than the traditional substorm wedge model would have predicted; by 0833 UT they had extended near the dawn and dusk magnetopause flanks. However, as shown by *Lu* [2000], the part of field-aligned currents due to the divergence of ionospheric Hall currents appeared to be more consistent with the traditional substorm current wedge, which evolved into a pair of upward and downward currents right after the substorm onset that were more confined to the x axis. Overall, Plate 1 shows that the magnetospheric source region of auroral precipitation has shifted tailward as well as duskward, from the inner central plasma sheet at the substorm onset to the duskside low-latitude boundary layer by the end of the expansion phase; the magnetospheric source region for the substorm-related field-aligned current, on the other hand, seems to be much closer to the Earth (extending from -6 to -30 R_E), and the peaks of current density remained nearly steady around geosynchronous altitude.

Plate 2 shows similar auroral UV images in the polar ionosphere as well as in the equatorial magnetosphere at 0748 UT (right after the substorm onset) and 0833 UT (near the end of the expansion phase), respectively, but with overlays of the corresponding electric potential contours. The ionospheric electric potential was plotted in the corotating frame of reference, whereas the magnetospheric electric potential was plotted in an inertial frame in the GSM coordinates. The corotation potentials at 110 km altitude were calculated at each AMIE grid point in apex magnetic coordinates [*Richmond*, 1995], taking into account the offset between the magnetic and geographic poles. The corotation potential at the geographic pole was arbitrarily set to zero. The sum of electric potentials in the corotating frame derived from AMIE and the corotation potentials was then mapped to the equatorial plane. Such an electric potential distribution in the inertial frame represents more realistically the steady state magnetospheric plasma flow trajectory [*Maynard et al.*, 1995]. It should be pointed out that the inductive electric field effect has not been taken into account in the mapped potential distribution, nor the field-aligned potential drop. As discussed in the next section the inductive electric fields are of the similar magnitude as electrostatic fields right after the substorm onset, but become much smaller than electrostatic fields during the late expansion phase.

The most distinct feature in ionospheric convection during this particular substorm was the development of an isolated convection cell: It evolved near midnight right after the substorm onset and then intensified and gradually merged with the preexisting dusk cell as the substorm proceeded [*Lu et al.*, 1998]. In the magnetospheric equatorial plane, plasmas had a roughly circular drift path in the near-Earth region owing to the corotation, and the last closed drift path in this case was at $L = \sim 3\ R_E$. This last closed path has been considered as the plasmapause [e.g., *Doe et al.*, 1992]. At the beginning of the substorm expansion phase (0748 UT), plasmas drifted roughly earthward in the region tailward of X = -4 R_E and duskward of $Y = 10\ R_E$, and plasmas drifted tailward near the dawn flank. By the end of the expansion (0833 UT), however, a relatively narrow region of tailward flow between 10 and 18 R_E in the y axis was found to be embedded inside the earthward flow region. Comparing the mapped auroral precipitation with the convection distribution in the equatorial plane, we found that the inner edge of the auroral precipitation was located just outside of the plasmapause. At 0833 UT the bright auroral emissions mapped to the narrow tailward flow region on the duskside, and the brightest aurora appeared to be located at the boundary between the earthward and tailward flows near the dusk flank. The bright discrete auroras shown at 0833 UT

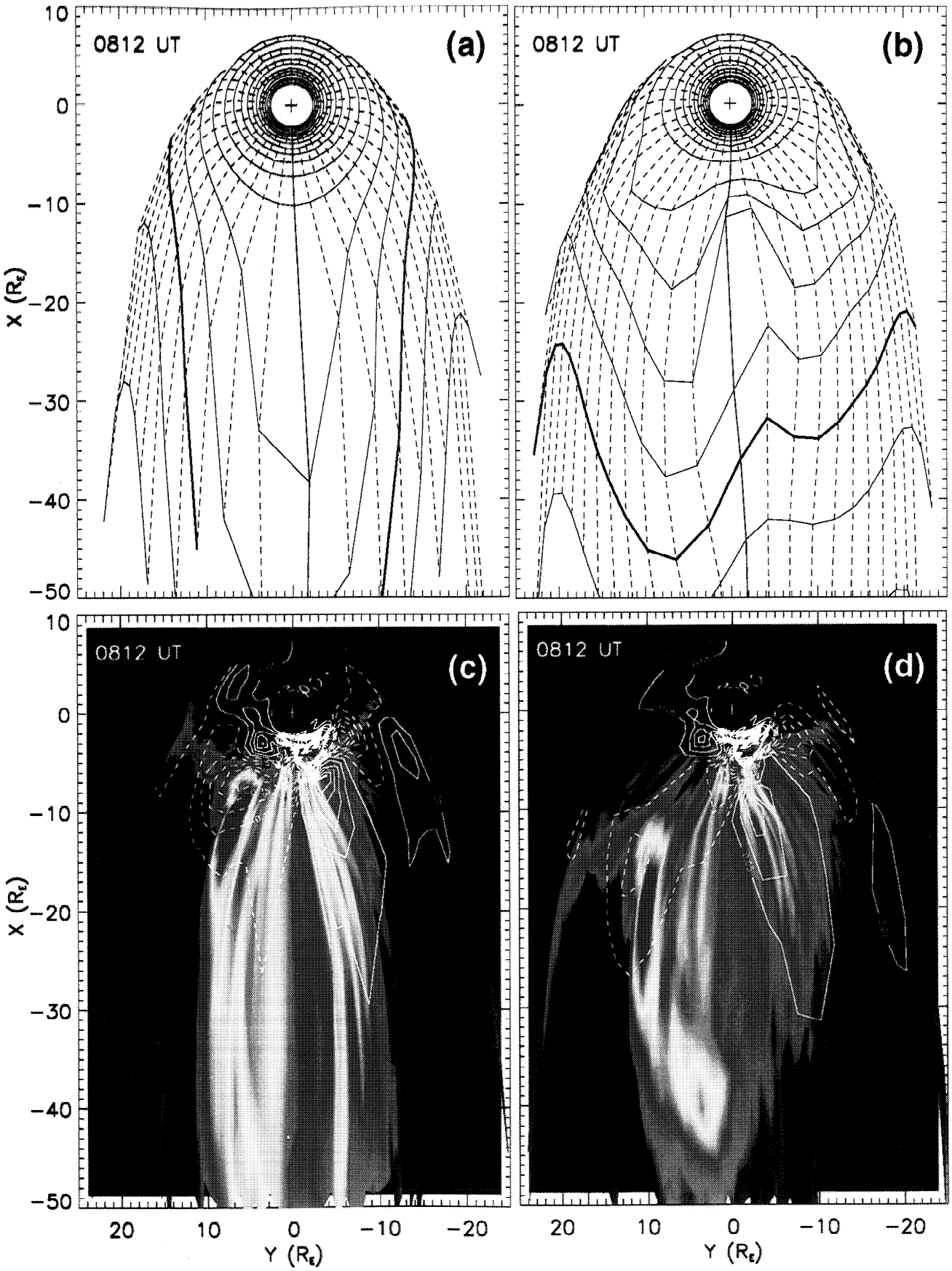

Plate 3. (a, b) Equatorial maps of AMIE grid mesh using the different magnetic field models (with the T96 model in Plate 3a and the modified model in Plate 3b). The heavy solid lines correspond to the 75° MLAT circle in the polar ionosphere. (c, d) Equatorial maps of auroral UV images and field-aligned currents using the different models (the T96 model in Plate 3c and the modified model in Plate 3d).

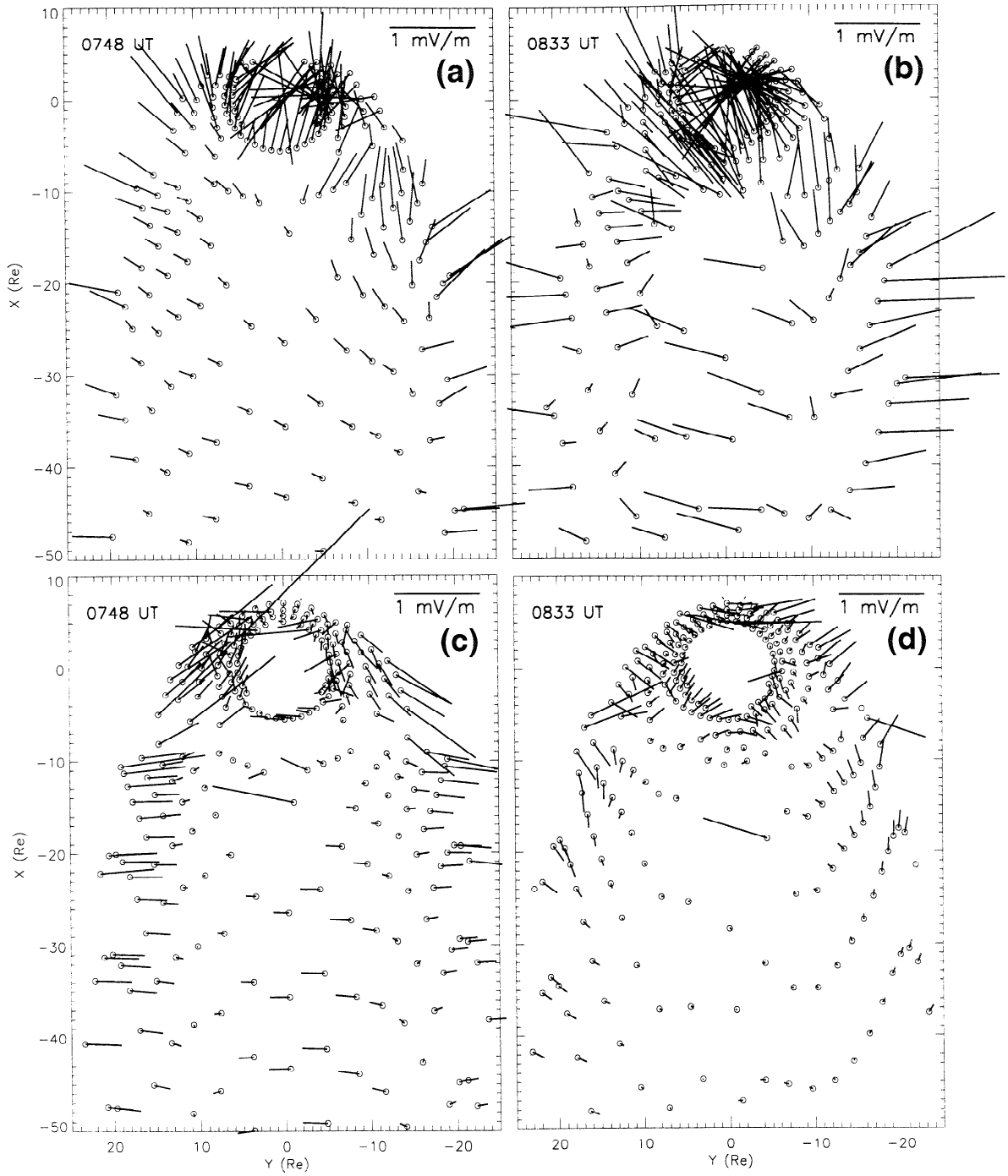

Figure 2. Projections in the GSM x-y plane of (a) electrostatic fields at 0748 UT, (b) electrostatic fields at 0833 UT, (c) inductive electric fields at 0748 UT, and (d) inductive electric fields at 0833 UT.

are often caused by accelerated precipitating electrons of ~10 keV in energy. Owing to the absence of polar-orbiting satellite observations during this event, we are unable to specify the field-aligned potential drops over the discrete auroral zone. Nevertheless, if we had included the upward field-aligned potential drop in the mapping, the flow shear would become steeper at the reversal boundaries surrounding this narrow tailward flow region.

3. Discussion

Mapping of substorm-related auroral precipitation and field-aligned currents has an important implication regarding where in the magnetosphere energy is dissipated through the manifestation of substorm disturbances. This study shows that the inner magnetotail, and particularly near geosynchronous altitude, is an important source region for both ionospheric auro-

ral precipitation and field-aligned currents at the early stage of the substorm expansion phase. Energetic particle injections are commonly observed in the inner magnetosphere by geosynchronous satellites, and they are considered to be an important indicator of substorm onset [e.g., *Parks and Winckler*, 1968; *McIlwain*, 1974; *Reeves et al.*, 1996; *Birn et al.*, 1997]. By examining simultaneously auroral X rays measured by high-altitude balloons and equatorial energetic electron fluxes of 50 keV to 1 MeV measured by the geosynchronous satellite ATS 1, *Parks* [1970] found that enhanced electron fluxes in the inner magnetosphere are strongly correlated with the enhanced precipitating electron fluxes in the ionospheric auroral zone. Our mapping results can therefore be interpreted as an indirect evidence in support of such a correlation.

Our study demonstrates that near the end of the expansion phase auroral surges mapped to a narrow region of tailward plasma flow between 10 and 18 R_E on the y axis, which is embedded in a much wider region of dominantly earthward flows. Because there were no satellites passing over the surge region in the ionosphere during the substorm, we are unable to identify the characteristics of precipitating particles. Nonetheless, the mapped location in the equatorial plane appears to be consistent with the expected inner LLBL or LLBL-CPS interface region. The association between the auroral surge and the LLBL-CPS interface region where large velocity shears exist seems to be in good agreement with the boundary layer dynamo model [*Rostoker*, 1996] which considers the KHI associated with the large velocity shear as the generation mechanism of enhanced auroral precipitation near the poleward edge of the auroral oval. Our mapping results are consistent with the work of *Henderson et al.* [1994], who linked the source region of the duskside horn-like structures during the late expansion phase to the LLBL and suggested boundary layer dynamics as a plausible mechanism for such auroral activations.

Our study also shows a clear departure of the magnetospheric source region of auroral precipitation from that of field-aligned currents shortly after the substorm onset. The initial auroral brightening at the substorm onset was related to processes at the inner edge of the plasma sheet. This is consistent with the findings of *Pulkkinen et al.* [1995, 1998] and *Frank et al.* [1998]. As the expansion phase progressed, the source region of the main auroral emissions was observed to move toward the duskside magnetospheric boundary in the vicinity of the LLBL, indicating different magnetospheric processes had taken place. The source region of field-aligned currents, on the other hand, remained nearly in the same place at the inner edge of the plasma sheet throughout the expansion phase. The apparently different magnetospheric source regions imply that the processes that produce energetic precipitating particles are not the same ones that generate the strongest magnetic perturbations in the magnetosphere. Our field-aligned current mapping led to a different conclusion than that of *Pulkkinen et al.* [1998], who claimed that the initial field-aligned currents couple to the midtail region at $X = -20 \sim -30\ R_E$ and interpreted the mapping result as an evidence of the midtail reconnection. However, it should be noted that Pulkkinen et al. did not actually map field-aligned currents; instead, they mapped the ionospheric locations associated with the largest ground magnetic perturbations, which do not correlate directly with field-aligned currents.

Substorm processes are highly dynamic. Magnetospheric electric and magnetic fields during substorms are thus strongly time-dependent. To investigate how important the inductive electric fields are compared to electrostatic fields, Figure 2 shows the distributions of both electrostatic fields (top) and the inductive electric fields (bottom) at 0748 UT and 0833 UT, respectively. For the sake of clarity, we plot out only those electric field vectors outside of 5 R_E from the Earth. Electrostatic fields were calculated from the gradient of the mapped electric potential patterns shown in Plate 2. The inductive electric fields E_{ind} were estimated based on the equatorial velocity V of a given magnetic field line. More specifically, we estimated the displacement δX of each field line that had the same ionospheric footprint during a time interval δt($\delta t = 3$ min in this case, that is, from 0748 UT to 0751 UT and from 0833 UT to 0836 UT), and the inductive velocity is thus $V = \delta X/\delta t$. $-V \times B$ gives rise to E_{ind}, where B is the magnetic field at the corresponding equatorial location. Only the GSM x-y projection of E_{ind} is plotted in Figure 2. By comparing the top and bottom projections, one can see that at the beginning of the expansion phase (0748 UT) the magnitude of the inductive electric field was comparable to or even larger than the magnitude of electrostatic field. As a result of the magnetic field dipolarization, the inductive electric fields in the CPS were in the same dawn-to-dusk direction as electrostatic fields, and thus enhanced the earthward convection. Near the dawn and dusk flanks, however, the inductive electric fields pointed from dusk to dawn due to the further stretching of field lines outside of the substorm current wedge. Such a distortion in magnetic fields during the expansion is shown in Plate 3. Recently, *Toivanen et al.* [1998] found that the inductive electric fields are comparable in magnitude but opposite in sign to the electrostatic fields during the substorm growth phase. In that study, electrostatic fields were obtained through the mapping of the empirical Heppner-Maynard potential pattern. At the late stage of the expansion phase (0833 UT), however, the inductive fields became less important compared to electrostatic fields (except in the middle of the CPS where the field dipolarization was probably still going on). The inductive electric fields were relatively weak compared to electrostatic fields inside geosynchronous orbit during the entire expansion phase, where electrostatic fields were essentially associated with corotation and were earthward with a magnitude of $\sim$1 mV/m.

The accuracy of the magnetospheric mapping de-

pends strongly on the accuracy of the magnetic field model used in mapping. To illustrate the effect of the different magnetic field models on field line mapping, we show in Plate 3 the mapping results using the T96 model and the modified model, respectively. Plates 3a and 3b show the mapping of AMIE grid mesh, which is uniform in ionospheric polar magnetic coordinates. The heavy solid lines in both images correspond to the 75° MLAT circle in the polar ionosphere. The T96 model has a tail-like configuration and is roughly symmetric around the x axis. The modified model, on the other hand, shows a clear distortion, where the ionospheric footprints close to midnight maps to relatively close to the Earth while those near dawn and dusk map relatively tailward. Such a distortion is attributed to the effect of the substorm wedge currents which play a dominant role in magnetic field line dipolarization during the expansion phase. The effect of the different magnetic field models on mapping is rather striking by comparing the same wobble-corrected auroral images shown in Plates 3c and 3d. For example, the brightest arc that mapped to X = -20 R_E using the modified model would otherwise correspond to X = -10 R_E if using the T96 model. Near the x axis, auroral emissions around -40 R_E would be mapped to tailward of -50 R_E (beyond the plotted range). In comparison, the mapping of field-aligned currents has relatively a lesser dependence on the magnetic field models because substorm-related field-aligned currents in the equatorial magnetosphere are concentrated much closer to the Earth. However, there is a noticeable difference between the mapped duskside wedge currents using the two different magnetic field models.

Although the magnetic field model used in this study showed a good agreement with the GOES data [*Lu et al.*, 1999], it was not tested beyond geosynchronous altitude owing to the lack of satellite observations. Therefore the features that map to the region tailward of 10 R_E may be subject to some degree of uncertainty.

4. Summary

We have presented in this study the first direct comparison of large-scale field-aligned current distributions and auroral UV images during the substorm expansion phase. Such comparison allows us to examine the relationship between auroral precipitation and field-aligned currents in a global context. It is found that the bright auroras generally coincide with upward field-aligned currents. However, the brightest discrete auroras tend to lie between the large-scale upward and downward field-aligned currents derived from AMIE. This probably is due to the fact that AMIE currently is unable to resolve the fine structures often associated with discrete auroras. With the aid of an improved time-dependent magnetic field model, we also examine the magnetospheric source regions of field-aligned currents and auroral precipitation during the substorm. Our equatorial mapping shows that the initial auroral brightening at the substorm onset appears to originate in the inner central plasma sheet at $X = -5 \sim -7R_E$. As the substorm progresses, the source region of auroral precipitation moves tailward and gradually toward the nightside dusk flank. The corresponding magnetospheric source region of substorm-related field-aligned currents, on the other hand, is relatively confined in the near-Earth region. Although the mapped field-aligned currents show a spatial expansion and an increase in magnitude during the expansion phase, their current densities peak around geosynchronous altitude. In contrast to the ionospheric field-aligned currents (as well as the UV auroral emissions) which show a poleward progression, the equatorial mapping of the substorm current system does not appear to move correspondingly tailward during the expansion phase, due in part to the dipolarization of the magnetic fields and in part to the relatively smaller mapping factor for those features at higher latitudes.

Acknowledgments. The ground magnetometer data used in this study were provided by T. Hughes at the Canadian Space Agency, L. Hakkinen at the Finnish Meteorological Institute, T. Moretto at the Danish Meteorological Institute, L. Morris at the National Geophysical Data Center of NOAA, K. Yumoto and the STEL at Nagoya University, G. van Beek of the Geological Survey of Canada, J. Posch at Augsburg College, D. Milling at the University of York, O. Troshichev at the Arctic and Antarctic Research Institute in Russia, K. Hayashi at the University of Tokyo in Japan, A. T. Weatherwax at the University of Maryland, G. Burns at the Atmospheric and Space Physics group at the Australian Antarctic Division, M. Pinnock at the British Antarctic Survey, V. Papitashvili at the University of Michigan, C. Maclennan at Bell Laboratories of Lucent Technologies, A. S. Potapov and S. I. Nechaev at the Institute of Solar-Terrestrial Physics at Irkutsk Observatory, and A. Zaitzev and V. Odintzov at IZMIRAN in Russia. The Wind magnetometer data were retrieved from the NASA CDAWeb database. The authors thank G. Rostoker for many helpful discussions. G. L. was supported in part by the NSF Space Weather program, and by the NASA Space Plasma Theory and ISTP/SEC Guest Investigator programs. D. L. was supported by NASA grant NAG5-7683.

Janet G. Luhmann thanks Howard J. Singer and another referee for their assistance in evaluating this paper.

References

Baker, D. N., T. I. Pulkkinen, V. Angelopoulos, W. Baumjohann, and R. L. McPherron, Neutral line model of substorms: Past results and present view, *J. Geophys. Res., 101*, 12,975, 1996.

Birn, J., and M. Hesse, Details of current disruption and diversion in simulations of magnetotail dynamics, *J. Geophys. Res., 101*, 15,345, 1996.

Birn, J., M. F. Thomsen, J. E. Borovsky, G. D. Reeves, D. J. McComas, and R. D. Belian, Characteristic plasma properties of dispersionless substorm injections at geosynchronous orbit, *J. Geophys. Res., 102*, 2309, 1997.

Brittnacher, M., M. Fillingim, G. Parks, G. Germany, and J. Spann, Polar cap area and boundary motion during substorms, *J. Geophys. Res., 104*, 12,251, 1999.

Doe, R. A., M. B. Moldwin, and M. Mendillo, Plasma-

pause morphology determined from an empirical ionospheric convection model, *J. Geophys. Res., 97*, 1151, 1992.

Eastman, T. E., G. Rostoker, L. A. Frank, C. Y. Huang, and D. G. Mitchell, Boundary layer dynamics in the description of magnetospheric substorms, *J. Geophys. Res., 93*, 14,411, 1988.

Elphinstone, R. D., J. S. Murphree, D. J. Hearn, W. Heikkila, M. G. Henderson, L. L. Cogger, and I. Sandahl, The auroral distribution and its mapping according to substorm phase, *J. Atmos. Terr. Phys., 55*, 1741, 1993.

Feldstein, Y. I., and Y. I. Galperin, The auroral luminosity structure in the high-latitude upper atmosphere: Its dynamics and relationship to the large-scale structure of the Earth's magnetosphere, *Rev. Geophys., 23*, 217, 1985.

Frank, L. A., J. B. Sigwarth, and W. R. Paterson, High-resolution global images of Earth's auroras during substorms, in *Substorm-4*, edited by S. Kokubun and Y. Kamide, pp. 3-8, Kluwer Acad., Norwell, Mass., 1998.

Fujii, R., R. A. Hoffman, P. C. Anderson, J. D. Craven, M. Sugiura, L. A. Frank, and N. C. Maynard, Electrodynamic parameters in the nighttime sector during auroral substorms, *J. Geophys. Res., 99*, 6093, 1994.

Henderson, M. G., J. S. Murphree, and G. D. Reeves, The activation of the dusk-side and the formation of north-south aligned structures during substorms, in *Proceeding of the Second International Conference on Substorms*, edited by J. R. Kan, J. D. Craven, and S.-I. Akasofu, pp. 37-42, Univ. of Alaska, Fairbanks, 1994.

Lu, G., A synthetic view of the magnetospheric-ionospheric current system associated with substorms, in *Magnetospheric Current Systems*, edited by S. Ohtoni et al., pp. 199-207, *Geophys. Monogr. Ser.*, vol. 118, AGU, Washington, D. C., 2000.

Lu, G., A. D. Richmond, Y. Kamide, D. Lummerzheim, M. Brittnacher, and G. Parks, Global ionospheric convection during substorm expansion, in *Substorm-4*, edited by S. Kokubun and Y. Kamide, pp. 617-622, Kluwer Acad., Norwell, Mass., 1998.

Lu, G., N. A. Tsyganenko, A. T. Y. Lui, H. J. Singer, T. Nagai, and S. Kokubun, Modeling of time-evolving magnetic fields during substorms, *J. Geophys. Res., 104*, 12,327, 1999.

Lui, A. T. Y., Current disruption in the Earth's magnetosphere: Observations and models, *J. Geophys. Res., 101*, 13,067, 1996.

Lui, A. T. Y., and J. R. Burrows, On the location of auroral arcs near substorm onsets, *J. Geophys. Res., 83*, 3342, 1978.

Lummerzheim, D., M. Brittnacher, D. Evans, G. A. Germany, G. K. Parks, M. H. Rees, and J. F. Spann, High time resolution study of the hemispheric power carried by energetic electrons into the ionosphere during the May 19/20, 1996 auroral activity, *Geophys. Res. Lett., 24*, 987, 1997.

Marklund., G. T., et al., Observations of the electric field fine structure associated with the westward traveling surge and large-scale auroral spirals, *J. Geophys. Res., 103*, 4125, 1998.

Maynard, N. C., W. F. Denig, and W. J. Burke, Mapping ionospheric convection patterns to the magnetosphere, *J. Geophys. Res., 100*, 1713, 1995.

McIlwain, C. E., Substorm injection boundary, in *Magnetospheric Physics*, edited by B. M. McCormac, pp. 143-154, D. Reidel, Norwell, Mass., 1974.

McPherron, R. L., C. T. Russell, and M. Aubry, Satellite studies of magnetospheric substorms on August 15, 1968, 9, Phenomenological model for substorms, *J. Geophys. Res., 78*, 3131, 1973.

Parks, G. K., The acceleration and precipitation of Van Allen outer zone energetic electrons, *J. Geophys. Res., 75*, 3802, 1970.

Parks, G. K., and J. R. Winckler, Acceleration of energetic electrons observed at the synchronous altitude during magnetospheric substorms, *J. Geophys. Res., 73*, 5786, 1968.

Pulkkinen, T. I., D. N. Baker, R. J. Pellinen, J. S. Murphree, and L. A. Frank, Mapping of the auroral oval and individual arcs during substorms, *J. Geophys. Res., 100*, 21,987, 1995.

Pulkkinen, T. I., et al., Two substorm intensifications compared: Onset, expansion, and global consequences, *J. Geophys. Res., 103*, 15, 1998.

Reeves, G. D., M. G. Henderson, P. S. McLachlan, R. D. Belian, R. H. W. Friedel, and A. Korth, Radial propagation of substorm injections, in *Third International Conference on Substorms, Eur. Space Agency Spec. Publ., ESA SP-389*, 579, 1996.

Richmond, A. D., Ionospheric electrodynamics using magnetic apex coordinates, *J. Geomagn. Geoelectr., 47*, 191, 1995.

Richmond, A. D., and Y. Kamide, Mapping electrodynamic features of the high-latitude ionosphere from localized observations: Technique, *J. Geophys. Res., 93*, 5741, 1988.

Rostoker, G., Phenomenology and physics of magnetospheric substorms, *J. Geophys. Res., 101*, 12,955, 1996.

Rostoker, G., and T. Eastman, A boundary layer model for magnetospheric substorms, *J. Geophys. Res., 92*, 12,187, 1987.

Samson, J. C., D. D. Wallis, T. J. Hughes, F. Creutzberg, J. M. Ruohoniemi, and R. A. Greenwald, Substorm intensifications and field line resonances in the nightside magnetosphere, *J. Geophys. Res., 97*, 8495, 1992.

Shiokawa, K., W. Baumjohann, and G. Haerendel, Breaking of high-speed flow and azimuthal pressure gradient as driving forces of substorm currents, in *Substorm-4*, edited by S. Kokubun and Y. Kamide, pp. 355-360, Kluwer Acad., Norwell, Mass., 1998.

Toivanen, P. K., H. E. Koskinen, and T. I. Pulkkinen, Mapping between the ionospheric and the tail electric fields in a time-dependent Earth's magnetosphere, *J. Geophys. Res., 103*, 9153, 1998.

Tsyganenko, N. A., Global quantitative models of geomagnetic field in the cislunar magnetosphere for different disturbance levels, *Planet. Space Sci., 35*, 1347, 1987.

M. Brittnacher and G. Parks, Department of Geophysics, University of Washington, P.O. Box 351650, Seattle, WA 98195-1650.

G. Lu, High Altitude Observatory, National Center for Atmospheric Research, 3450 Mitchell Lane, Boulder, CO 80301. (e-mail: ganglu@ucar.edu)

D. Lummerzheim, Geophysical Institute, University of Alaska, 903 Koyukuk Drive, Fairbanks, AK 99775-7320

(Received September 28, 1999; revised February 24, 2000; accepted February 28, 2000.)